The influence of temperature on the elastic properties of body-centered cubic reduced activation steels

Xiaojie Li [a,b], Stephan Schönecker [b,*], Xiaoqing Li [b,*], Jijun Zhao [c,*], Levente Vitos [b,d,e]

[a] Department of Physics, Taizhou University, Taizhou 318000, China
[b] Applied Materials Physics, Department of Materials Science and Engineering, KTH - Royal Institute of Technology, Stockholm SE-10044, Sweden
[c] Key Laboratory of Materials Modification by Laser, Electron, and Ion Beams (Dalian University of Technology), Ministry of Education, Dalian 116024, China
[d] Department of Physics and Astronomy, Division of Materials Theory, Box 516, SE-75120 Uppsala, Sweden
[e] Research Institute for Solid State Physics and Optics, P.O. Box 49, H-1525 Budapest, Hungary

HIGHLIGHTS

- A comprehensive picture of the temperature effect on the elastic properties of reduced activation steel is provided.
- Loss of long-range magnetic order, volume expansion and entropy are important in determining temperature-dependence elastic parameters.
- Alloying effects on the elastic properties differ in the magnetically ordered and disordered phases.
- A peculiar magneto-volume phenomenon on the equation of state in Fe is gradually removed by alloying or magnetic disordering.

GRAPHICAL ABSTRACT
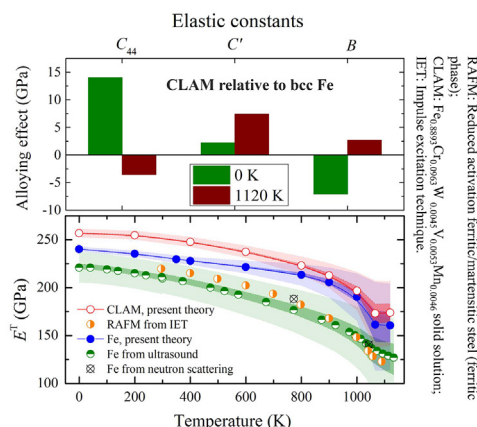
ARTICLE INFO

ABSTRACT

A first-principles based modeling approach to the effect of temperature on the isothermal single-crystal and poly-crystalline elastic parameters of Fe-rich solid solutions is reported. The approach integrates alloy theory for chemical and magnetic disorders with accessible experimental data for the equilibrium volume and ferro-magnetic phase transition, and is adopted to predict the temperature-dependent elastic parameters of the body-centered cubic phase of three reduced activation steels, CLAM/CLF-1, F82H, EUROFER97, considered as high-temperature material in power reactors. The predictions are assessed based on available experimental data for a reduced activation steel and both experimental and theoretical data for pure Fe. Alloying effects on the elastic constants relative to pure Fe are found to differ in the magnetically ordered and disordered phases. Contributions due to loss of long-range magnetic order, volume expansion, and entropy are important in determining the temperature dependence of the elastic parameters in all investigated materials. A previously reported, peculiar magneto-volume phenomenon on the equation of state in pure Fe is gradually removed by alloying and magnetic disordering, which requires particular attention when describing the thermo-chemical effects derived from the equation of state in Fe-rich solid solutions.

* Corresponding authors.
    E-mail addresses: stesch@kth.se (S. Schönecker), xiaoqli@kth.se (X. Li), zhaojj@dlut.edu.cn (J. Zhao).

1. Introduction

Reduced activation steels are derivatives of body-centered cubic (bcc), Fe-rich, Fe-Cr binary alloys with minor addition of low-activation elements, such as V, Mn, Ta, W, Si, and C. These grades are considered as candidate structural materials for first wall and breeding-blanket applications in fusion power reactors [1–3], where they will be subject to temperatures considerably above 300 K, and exposed to plasma particles and neutron irradiation. Operation in such extreme environments makes it vitally important to understand how their mechanical behavior degrades with temperature and/or irradiation. The technological challenge of designing reactors is compounded by the fact that the mechanical properties of structural materials mainly limit the temperature window of operation (approximately 620–820 K for reduced activation steels and somewhat higher in oxide-dispersion strengthened grades).

Among the quantities characterizing mechanical behavior, the knowledge of the elastic parameters is essential for alloy design, as these coefficients directly provide information about the mechanical response under various loading conditions. Furthermore, the elastic parameters are crucial for multi-scale modeling of mechanical properties including crystal plasticity [4,5] and phase-field models [6], modeling fracture [7,8] and solid solution hardening [9,10], and estimating dislocation core properties [11].

Where experimental data are missing or difficult to obtain, first-principles calculations can provide the necessary information, in addition to giving insight into microscopic mechanisms underlying the trends predicted or observed. First-principles modeling of temperature effects on the elastic parameters of Fe-based materials is, however, difficult. The treatment of magnetic excitations remains a serious challenge in the absence of a complete theory for itinerant electron magnetism [12,13]. Furthermore, the variety of chemical configurations and the large fraction of alloying elements present in real alloy systems can typically not be sufficiently captured in tangible simulation cells. The last decade has witnessed considerable development in modeling the free energy of α-Fe enabling some thermodynamic predictions [14–16]. These approaches remain, however, in most cases laborious and computationally challenging rather than being routine. The challenges mentioned practically limit the investigations of solute-induces changes in elastic parameters at finite temperature, and call for efficient, yet accurate, modeling approaches.

In this paper, we address these issues by combining first-principles alloy theory for chemical and magnetic disorders, as treated by the coherent-potential approximation (CPA) and disordered-local moment (DLM) model, respectively, with experimental data for the equilibrium volume and ferromagnetic phase transition. The modeling approach is applied to compute the isothermal single-crystal and polycrystalline elastic parameters of three reduced activation steels in the ferritic (bcc) phase. Their chemical compositions are $Fe_{0.8893}Cr_{0.0963}W_{0.0045}$ $V_{0.0053}Mn_{0.0046}$, $Fe_{0.9077}Cr_{0.0802}W_{0.0060}V_{0.0040}Mn_{0.0021}$, and $Fe_{0.8907}$ $Cr_{0.0949}W_{0.0033}V_{0.0066}Mn_{0.0045}$. These compositions are similar to those of three reference reduced activation steel grades (main alloying elements) termed CLAM/CLF-1, F82H, and EUROFER97, respectively [17,18]. Although these grades contain other substitutional or interstitial elements in low concentrations, which are not considered here, we adhere to these names for the sake of convenience. CLAM/CLF-1 (for brevity referred to as CLAM hereafter), F82H, and EUROFER97 were selected due to technology maturity. In order to assess the methodology, our results are compared to available experimental results for a reduced activation steel. However, due to the limited amount of data available, α-Fe is also included in the assessment, since for this system both theoretical and experimental data are available. We recently examined the zero-temperature properties of these grades in detail [19] and concentrate here on the effect of finite temperatures up to slightly above the magnetic ordering temperature.

2. Linear elasticity

Let $F = F(T, \boldsymbol{\varepsilon})$ be the Helmholtz free energy of a linear thermoelastic solid for given temperature T and Eulerian strain $\boldsymbol{\varepsilon}$. The isothermal single-crystal elastic constants C_{ijkl}^T are the expansion coefficients of the Helmholtz free energy in terms of the strain components evaluated at the reference state [20,21],

$$C_{ijkl}^T = \frac{1}{V_0} \left(\frac{\partial^2 F(T, \boldsymbol{\varepsilon})}{\partial \varepsilon_{ij} \partial \varepsilon_{kl}} \right)_T. \tag{1}$$

V_0 is the volume of the reference state. Subscripts $i, j, \ldots$ indicate Cartesian components and each goes over three values. The dependence of F on the volume of the reference state is not indicated explicitly.

Crystals of cubic symmetry possess three independent second-order elastic constants (SOECs), C_{1111}^T, C_{1122}^T, and C_{1212}^T. In contracted notation used henceforth ($C_{\alpha\beta}^T, \alpha, \beta = \{1\ldots6\}$), they are denoted C_{11}^T, C_{12}^T, and C_{44}^T, respectively. The tetragonal shear elastic constant is defined by $C^T = (C_{11}^T - C_{12}^T)/2$ and the Zener anisotropy ratio is $A_Z = C_{44}^T/C^T$.

Single-crystal elastic constants determined experimentally by dynamic methods resemble to a larger extent isentropic conditions provided the frequency of vibration is sufficiently high (as in ultrasound) [22]. A conversion from isentropic ($C_{\alpha\beta}^S$) to isothermal coefficients for crystals of cubic symmetry can be obtained via [23,24],

$$C_{11}^T = C_{11}^S - \Delta, \quad C_{12}^T = C_{12}^S - \Delta, \quad C_{44}^T = C_{44}^S, \tag{2}$$

where

$$\Delta = \frac{\beta \left(B^S\right)^2}{1 + \beta B^S}, \quad \beta = \frac{9V_0 T \alpha^2}{c_p}. \tag{3}$$

Here, α is the true coefficient of thermal expansion, c_p the specific heat capacity at constant pressure, and $B = (C_{11} + 2C_{12})/3$ the bulk modulus for either isothermal or isentropic coefficients. Since Δ is positive semi-definite, C_{11}^S and C_{12}^S have greater values at $T > 0$ than the isothermal counterparts, and the difference is an increasing function of temperature.

For isotropic polycrystalline aggregates, the (effective) shear modulus G can be obtained from the single-crystal elastic constants through averaging methods, and the Voigt-Reuss-Hill (VRH) scheme was mainly used here [25]. Several other averaging methods to define effective moduli exist, and the Hashin-Shtrikman bounds [26] are also employed to discuss our results. The (effective) Young modulus E and the Poisson ratio ν are related to B and G through $E = 9BG/(3B + G)$ and $\nu = (3B - 2G)/(6B + 2G)$. Note that the difference between isothermal and isentropic coefficients cancels for C_{44}, C', and G.

3. Modeling framework and computational details

Let $\mathcal{A}$ be a unary material, and $\mathcal{A}_{x_a} B_{x_b} \mathcal{C}_{x_c} \ldots$ a substitutionally disordered alloy, where $x_a, x_b, x_c \ldots$ denote the atomic fractions of alloy chemical species $\mathcal{A}, \mathcal{B}, \mathcal{C} \ldots$.

The description of the Helmholtz free energy $F = F(T, \boldsymbol{\varepsilon})$ is based on the adiabatic approximation, since magnetic, electronic, and vibrational excitations in solids are connected with different time scales, viz.

$$F = F_{\text{mag}} + F_{\text{el}} + F_{\text{vib}}. \tag{4}$$

The lattice dynamics correspond to the slow degree of freedom and should be described using a potential-energy surface equilibrated with respect to the fast, i.e., electronic and magnetic, degrees of freedom. In the harmonic or quasi-harmonic approximation, F_{vib} may be determined through calculation of the interatomic force constant matrix by means of, e.g., the small displacement method. This approach seems feasible as long as the number of atoms in the unit cell is small. If the alloy

state and/or static finite-temperature magnetic state itself is represented by a super cell, this approach is obviously much less feasible, rendering accurate phonon calculations for magnetic alloys generally difficult. Because of this computational and methodological challenge, we did not further consider the explicit lattice vibrational contribution, and approximate F by the partial magnetic and electronic contributions. Nevertheless, the thermal lattice expansion is considered as elaborated in Sec. 3.5.

We detail on the partial magnetic and electronic free energy contribution in the following subsections. Section 3.3 introduces two sets of isothermal elastic constants for the sake of discussion. As first-principles modeling of the finite-temperature excitations in the whole temperature interval considered is rather complicated, we partially employ experimental data including the thermal expansion.

3.1. Magnetic contribution

Our starting point are two well-established limits of the first-principles formulation of metallic magnets with rather localized magnetic moments, such as Fe [12]. On the one hand, we resort to the zero temperature ground state with total energy $E_{GS} = E_{GS}(\varepsilon)$, which is assumed to be magnetically ordered and described by spin density-functional theory (DFT) considering collinear spin ordering. For the magnetic materials considered here, bcc Fe orders ferromagnetically. Cr spins in Fe-rich, Fe-alloy align antiparallel to Fe spins, whereas Mn spins align parallel. W and V are only slightly spin-polarized by Fe and orient similar to Cr.

On the other hand, we draw upon the DLM formalism, which is a mean-field type electronic theory in the presence of static, random transverse spin fluctuations [27–29]. The DLM state can be directly related to the finite-temperature paramagnetic state above the magnetic ordering temperature. The total energy of a DLM paramagnet $E_{PM} = E_{PM}(\varepsilon)$ is most readily determined by means of Green's function based electronic structure methods as employed here (Sec. 3.6). Using its alloy analogy, the DLM state of material $\mathcal{A}$ is represented by an equimolar pseudo-binary alloy $\mathcal{A}^{\uparrow}_{0.5}\mathcal{A}^{\downarrow}_{0.5}$, composed of equal fractions of atoms with up spins ($\mathcal{A}^{\uparrow}$) and down spins ($\mathcal{A}^{\downarrow}$).

In order to investigate the material properties in between the limits of complete magnetic order and random magnetic disorder, we apply the partial DLM (PDLM) interpolation (or uncompensated DLM) [30,31]. The PDLM interpolation is easily illustrated by way of the alloy analogy. The pseudo-alloy representation of material $\mathcal{A}$ in a completely ordered, partially or fully magnetically disordered state is $\mathcal{A}^{\uparrow}_{1-\zeta}\mathcal{A}^{\downarrow}_{\zeta}$, where ζ is the pseudo-alloy concentration ($0 \leq \zeta \leq 0.5$), and the corresponding total energy is denoted $E_{PDLM} = E_{PDLM}(\varepsilon, \zeta)$. Obviously, $E_{GS} = E_{PDLM}(\cdot, 0)$ and $E_{PM} = E_{PDLM}(\cdot, 0.5)$ in the completely ordered limit ($\zeta = 0$) and fully disordered limit ($\zeta = 0.5$), respectively. A partially magnetically disordered state ($0 < \zeta < 0.5$) is interpreted as a magnetic state similar to a finite-temperature state below the magnetic ordering temperature.

The pseudo-alloy representation of the reduced activation steels considered was described as $(Fe^{\uparrow}_{1-\zeta}Fe^{\downarrow}_{\zeta})_{1-x-y-z-u}(Cr^{\uparrow}_{1-\zeta}Cr^{\downarrow}_{\zeta})_x W_y V_z Mn_u$. The magnetic elements Fe and Cr have identical pseudo-alloy concentrations on account of a single magnetic phase transition in their alloyed form. Although Mn is magnetic as well, a Mn pseudo-alloy is not considered due to its very low concentration in the compositions considered.

The magnetic free energy is,

$$F_{mag} = E_{PDLM} - TS_{mag}, \tag{5}$$

where the magnetic entropy

$$S_{mag}/k_B = 2\zeta \sum_{i=a,b,c\ldots} x_i \ln(1 + \mu_i) \tag{6}$$

is derived from the mean-field expression [32,33], and interpolates between the limits of complete magnetic order and random magnetic

disorder. μ_i stands for the magnitude of local magnetic moment (in units of Bohr magneton) of species i in the material, and k_B is the Boltzmann constant. For a pseudo-alloy, μ_i is that of the majority component $\mathcal{A}^{\uparrow}$.

3.2. Electronic smearing

Electronic excitations to the free energy are considered by way of smearing the Fermi-Dirac distribution [34,35]. We may formally define F_{el} as the energy difference between electronic smearing taken into account and not taken into account, viz.

$$F_{el} = F_{PDLM}(T, \varepsilon, \zeta) - E_{PDLM}(\varepsilon, \zeta). \tag{7}$$

Here, the T-dependence of F_{PDLM} enters through the Fermi-Dirac distribution and contains entropic effects.

Explicit calculations for pure Fe showed that electronic excitations constitute a minor effect on the elastic constants and can be neglected. For instance, for pure Fe at $T = 600$ K (Wigner-Seitz radius, $w = 2.657$ Bohr), electronic smearing increases C^T by approximately 1 GPa (or 2% change) and C^T_{44} by approximately 1 GPa (<1% change). The neglect is justified by alloy disorder effects on the electronic structure (chemistry and pseudo-alloying). For the sake of reducing the computational load, we did not further consider F_{el} in our finite-temperature calculations and all results presented in Secs. 4 and 5 were derived without considering electronic smearing.

3.3. Isothermal elastic constants: Two cases

Collecting the remainder of the partial contributions introduced above, we first define a partial free energy F_{mag} that is parametric in the pseudo-alloy concentration ζ as

$$\begin{aligned} F_{mag}(T, \varepsilon, \zeta) &= E_{PDLM}(\varepsilon, \zeta) - TS_{mag} \\ &\Rightarrow C^{T,\zeta}_{\alpha\beta}. \end{aligned} \tag{8}$$

Isothermal elastic constants derived from Eq. (8) are denoted by $C^{T,\zeta}_{\alpha\beta}$ and may be obtained for a general state in (T, V_0) space and for ordered, partially or fully magnetically disordered states. The purpose of defining this F_{mag} and $C^{T,\zeta}_{\alpha\beta}$ is, for instance, to establish the effect of losing long-range magnetic order on the elastic constants at constant reference volume, or to assess the effect of volume expansion on the elastic constants in the magnetically ordered state.

When thermal equilibrium at zero pressure determines reference volume [$V_0 = V_0(T)$] and magnetic state [$\zeta = \zeta(T)$] at some temperature T, we refer to $\mathscr{F}_{mag}(T, \varepsilon)$ defined by

$$\begin{aligned} \mathscr{F}_{mag}(T, \varepsilon) &\equiv F_{mag}(T, \varepsilon, \zeta(T)) \\ &\Rightarrow C^T_{\alpha\beta}. \end{aligned} \tag{9}$$

Volume expansion of the reference state is assumed implicitly, and any changes in volume may arise only from volumetric strain. Isothermal elastic constants derived from $\mathscr{F}_{mag}$ are denoted by $C^T_{\alpha\beta}$. In evaluating these, the effect of volume expansion via temperature-dependent reference-state volumes, and the magnetic contribution via the PDLM interpolation of the total energy and magnetic entropy are considered.

It is to be remarked that ζ is not a meaningful parameter of this model when completely ordered and fully magnetically disordered states are not stable for certain volumes or elastic strains, i.e., when self-consistent calculations converge into a non-magnetic state with zero local magnetic moment. This issue is avoided by considering domains of volumes and elastic strains where ferromagnetic and paramagnetic states are stable in self-consistent calculations.

The next section describes in more detail how the temperature is mapped to the pseudo-alloy concentration.

3.4. Temperature dependence of magnetic state

Modeling the magnetic energy E_{PDLM} due to gradual loss of long-range magnetic order requires establishing the relation between the pseudo-alloy concentration ζ and temperature T. This may be achieved on the basis of the normalized order parameter for the magnetic phase transition $m = M_s(T)/M_{s0} = f(\zeta)$, where M_s is the saturation magnetization, $M_{s0} \equiv M_s(0\mathrm{K})$ the zero temperature saturation magnetization, and $1 \geq m \geq 0$.

The magnetization is the order parameter in the case of a ferromagnet, and the magnetization curve connects m to T. Magnetization curves may be readily determined by solving a Heisenberg Hamiltonian with first-principles derived exchange parameters through classical Monte Carlo simulations. Previous research showed, however, that this approach does not reproduce the shape of the experimental magnetization curve at low temperatures due to use of classical Boltzmann statistics [36,37], while going beyond the Heisenberg Hamiltonian or Boltzmann statistics is beyond the scope of this paper. Therefore, we employ a simple analytical function [38],

$$m(\tau) = \left[1 - s\tau^{3/2} - (1-s)\tau^p\right]^{1/3}, \qquad 0 \leq \tau \leq 1, \tag{10}$$

to map the reduced temperature $\tau = T/T_{ord}$ to m, where T_{ord} denotes the magnetic ordering temperature. For $\tau \geq 1$, $m = 0$. s and p are parameters with values 0.35 and 5, respectively, determined in Ref. [38] for bcc Fe by fitting experimentally data to Eq. (10). In lack of experimental data, we adopted the same values for s and p for CLAM steel.

In practice, for a given $T \leq T_{ord}$, we first determine m via Eq. (10), then compute the zero temperature magnetization per unit cell, and finally determine by variation that ζ that gives a M_s to M_{s0} ratio equal to m. To a good approximation, $m = 1 - 2\zeta$.

We employed $T_{ord} = 1066$ K for pure Fe (experimental value is 1043 K), previously determined theoretically by us [39]. Using the mean-field approximation for the ordering temperature [40], we found that the Curie temperatures of Fe and CLAM steel slightly differ by -36 K, which is consistent with experimental observations for pure Fe and the Fe-Cr binary with $x \approx 10$ at.% Cr [41] (difference ≈ -21 K). For this reason, we used the same ordering temperature ($T_{ord} = 1066$ K) for CLAM as well.

We should remark that the mapping in Eq. (10) introduces a volume and strain dependence of ζ, as T_{ord} may depend on V_0 and $\boldsymbol{\varepsilon}$. Isothermal strain derivatives of F_{mag} or $\mathscr{F}_{mag}$ should thus take into account the variation of ζ with volume and strain under isothermal conditions. Our test calculations using the mean-field approximation for the magnetic ordering temperature showed that elastic constants derived from strain derivatives at constant ζ differ from those at constant T by at most 8 GPa. This is considered an acceptable error, and for the sake of reducing the computational load, we assumed volume and strain independent T_{ord} and ζ in our finite-temperature calculations presented in Sec. 4.

3.5. Thermal expansion

The thermal lattice expansion was considered on the basis of the Grüneisen theory for the true linear coefficient of thermal expansion [42,43]. Some experimental linear expansion coefficients are available for CLAM steel at elevated temperatures (573–973 K) in Ref. [44]. Using a least-square method, we fitted these experimental data to the Grüneisen expression [43] in order to determine the linear coefficient of thermal expansion in an extended temperature interval. The resulting Grüneisen plot for CLAM shown in Fig. 1 follows the experimental data in 573–973 K closely. However, the expansion coefficient at low temperature appears to be too low (in a Debye model, the Debye temperature would be too high indicating a too stiff lattice), but the fit could be improved given additional experimental data
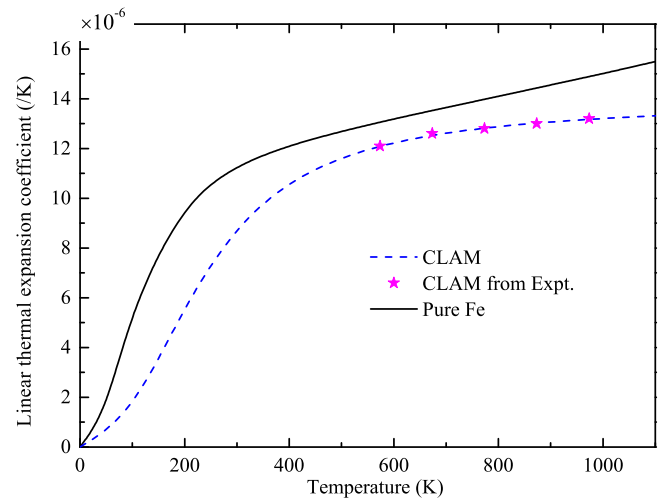

Fig. 1. Grüneisen plots (lines) of the linear coefficient of thermal expansion for CLAM steel compared to Fe (reproduced from Ref. [43]). The CLAM curve was obtained by fitting the available experimental data reported in [44] to the Grüneisen expression [43]. Note that the magnetic phase transition may produce changes in volume near T_{ord} that are not captured by the Grüneisen theory.

points. In lack of experimental data and due to similar composition, we adopted the same linear expansion coefficients for F82H and EUROFER steels.

In the case of Fe, we employed the result of Nix and MacNair [43], who fitted experimental data measured in the temperature interval of 92–958 K to the Grüneisen expression. The Grüneisen plot for Fe is reproduced in Fig. 1.

Previously reported averaged expansion coefficients for Fe-rich ferrite [45] allow to verify our results obtained from the Grüneisen theory, since the chemical compositions of CLAM (main alloying elements) and $Fe_{90}Cr_{10}$ are close. The direct experimental assessment [45] shows that the linear thermal expansion coefficient, averaged between room temperature and 865 K, decreases by approximately -1.8×10^{-6} K^{-1} upon alloying Fe with 10 at.% Cr. From the Grüneisen plots we determined the temperature-averaged coefficients (293–865 K) of 12.9×10^{-6} K^{-1} and 11.7×10^{-6} K^{-1} for Fe and CLAM, respectively. With a change of -1.2×10^{-6} K^{-1}, we find ourselves in good qualitative agreement with the results of Hull et al. [45].

All theoretical, finite temperature Wigner-Seitz radii were obtained by rescaling the calculated equilibrium Wigner-Seitz radii (in the magnetically ordered phase) with the above linear thermal expansion coefficients.

3.6. Methodological details and electronic structure method

For clarity, we summarize the principal steps necessary to determine $\mathscr{F}_{mag}(T, \boldsymbol{\varepsilon})$ for any of the considered materials and whose theoretical equilibrium volume is assumed to be determined. For a chosen temperature T, first determine the reference state volume $V_0(T)$ (Sec. 3.5). Second, determine the order parameter m and the pseudo-alloy concentration ζ of the pseudo-alloy representing the material's magnetic state at T (Secs. 3.1 and 3.4). Third, perform total-energy calculations for the pseudo-alloy, using alloy theory as detailed below, for a set of strains $\boldsymbol{\varepsilon}$ applied to the reference state, considering the Fermi-Dirac distribution at T (Sec. 3.2). Finally, extract the local magnetic moments and add the (strain-dependent) "$-TS_{mag}$" term (Sec. 3.1). The steps to determine $F_{mag}(T, \boldsymbol{\varepsilon}, \zeta)$ are similar except that V_0 and T are treated as independent variables (Sec. 3.3). The following part describing the determination of the elastic constants applies to both $C_{\alpha\beta}^T$ and $C_{\alpha\beta}^{T,\zeta}$.

The three cubic elastic constants, or combinations thereof, were obtained by applying homogeneous strains to the bcc crystal structure, and fitting the resulting energy change as a function of distortion. Specifically, we employed volume-conserving orthorhombic and monoclinic strains to calculate C^T and C_{44}^T, respectively (for details, we refer the reader to Ref. [46]). The bulk modulus of the bcc phase (at V_0, which does not need to coincide with the minimum of the partial free energy) was derived from a third-order Birch-Murnaghan equation of state (EOS) [47]. Default fitting comprised seven total energy data for a Wigner-Seitz radius in the range of 2.58–2.70 Bohr (equi-distant steps of 0.02 Bohr). These settings were deliberately chosen after careful testing as to maintain a high goodness of fit; cf. discussion in Sec. 5.3.

All present DFT calculations were performed using the all-electron, exact muffin-tin orbitals (EMTO) method [48–50]. Scalar-relativistic, self-consistent calculations were carried out using the local-density approximation by Perdew and Wang [51], whereas the total energy was determined via the full charge-density technique [52] in combination with the Perdew-Burke-Ernzerhof gradient-corrected functional [53]. The soft-core basis set included the default s, p, d, and f orbitals. The CPA [54–56] was employed to describe compositional disorder (including the DLM state and the PDLM interpolation). An electrostatic correction to the single-site CPA was described using the screened impurity model with screening parameter of 0.602 [57,58]. Short-range order effects and local-lattice relaxation were not considered due to single-site nature of the CPA. This approximation is also motivated by the relatively low concentrations of the alloying additions. The Brillouin zones were sampled by approximately 20,000–27,000 uniformly distributed k-points to ensure the required accuracy in the single-crystal elastic constant calculations.

4. Results

We begin by examining the isothermal elastic properties of the reduced activation steels in the limits of complete magnetic order at 0 K and random magnetic disorder at 1120 K. We then turn to their temperature-dependent elastic properties in the range of 0 to 1120 K. The temperature of 1120 K was chosen on account of available experimental data used to discuss the modeling approach (Sec. 5). For reference and to establish alloying trends, we include results for pure Fe.

4.1. Elastic properties of reduced activation steels in the magnetically ordered and paramagnetic states

Table 1 lists the isothermal theoretical single-crystal elastic constants and derived polycrystalline moduli for bcc CLAM, F82H, and EUROFER97 at 0 and 1120 K. We first observe that the solid solution description of these three reduced activation steels results in rather similar elastic properties due to similar chemical compositions.

Choosing $C_{\alpha\beta}^T$ of CLAM as example, the 1120 K and 0 K values for C_{11}^T differ strongly by 107 GPa, whereas C_{12}^T and C_{44}^T are rather similar. C^T at 1120 K decreases to about a third of the 0 K value, whereas the Zener ratio triples. The polycrystalline moduli B^T, G^T, and E^T at 1120 K are approximately 21%, 34%, and 32% lower, respectively, than their zero temperature values in the ferromagnetic state, and both ν^T and B^T/G^T increase moderately by 11% and 17%, respectively.

For reference, we also list our results for pure Fe in the paramagnetic and ferromagnetic states in Table 1. We notice that the present theoretical data for pure Fe are similar to those published previously [15,19,59,60]. Minor differences arise due to the use of theoretical or experimental lattice parameters, different exchange-correlation functionals, fitting with different EOSs, or inclusion of longitudinal spin fluctuations in the paramagnetic state (Refs. [59, 60]).

Relative to paramagnetic Fe at 1120 K, the compositional effect of the main alloying elements characteristic of the three reduced activation steels is a change of C_{11}^T, C_{12}^T, C_{44}^T, and C^T by at most 8%, −2%, −3%, and 36%, respectively. In contrast, the three isotropic moduli B^T, G^T, and E^T are larger in the steels, in particular Young's modulus. Both ν^T and B^T/G^T differ by approximately 5%.

We find that the compositional trends on the elastic constants and moduli differ in the magnetically ordered and disordered phases. For instance, the three steels have a larger (smaller) C_{11}^T than Fe in the paramagnetic (magnetically ordered) phase, while C_{12}^T of Fe is smaller than that of the steels at both 0 K and 1120 K. In addition, the magnitude of the alloying effect in the paramagnetic phase can be very different from that in the magnetically ordered phase, e.g., as evident in the case of C_{44}^T.

For later purpose (Sec. 5.2), we determined all the elastic parameters in the magnetically disordered state at zero temperature and corresponding theoretical equilibrium volume. These values are listed in Table 1 and denoted by $C^{T,\xi=1}$.

Table 1

Isothermal single-crystal elastic constants and polycrystalline elastic moduli for bcc CLAM, F82H, and EUROFER97 from present theory. Present theoretical for Fe, and previous experimental data for Fe and a RAFM steel are shown for comparison. Temperature T (in units of K), Wigner-Seitz radius w (in units of Bohr), and magnetic state (MS; ordered ground state or disordered paramagnetic state) specify the conditions under which the calculations were performed or the experiments (Expt.) were conducted. Elastic parameter type indicates C^T or $C^{T,\xi}$ (matrix indices omitted). All elastic parameters are in units of GPa.

Material	State				Elastic parameter									
	T	w	MS	Type	C_{11}	C_{12}	C_{44}	C'	A_z	B	G	E	ν	B/G
CLAM	1120	2.684	disord.	C^T	178	122	118	28	4.2	140	67	174	0.29	2.1
	0	2.654	ord.	C^T	285	125	120	80	1.5	178	102	257	0.26	1.8
	0	2.654	disord.	$C^{T,\xi=1}$	200	150	133	25	5.3	167	69	183	0.32	2.4
F82H	1120	2.685	disord.	C^T	174	122	118	26	4.5	139	65	170	0.30	2.1
	0	2.655	ord.	C^T	282	125	119	79	1.5	177	101	254	0.26	1.8
	0	2.655	disord.	$C^{T,\xi=1}$	197	149	133	24	5.5	165	68	180	0.32	2.4
EUROFER97	1120	2.683	disord.	C^T	177	122	118	27	4.3	140	66	172	0.30	2.1
	0	2.653	ord.	C^T	284	125	120	80	1.5	178	102	257	0.26	1.8
	0	2.653	disord.	$C^{T,\xi=1}$	200	150	133	25	5.3	166	69	182	0.32	2.4
RAFM, Expt. [64] [§]	~1100	n/a	disord.	C^T	n/a	n/a	n/a	n/a	n/a	n/a	51	123	n/a	n/a
Fe	1120	2.677	disord.	C^T	166	124	121	21	5.8	138	62	161	0.31	2.2
	0	2.642	ord.	C^T	289	134	106	78	1.4	185	94	240	0.28	2.0
	0	2.642	disord.	$C^{T,\xi=1}$	192	157	140	17	8.1	168	64	170	0.33	2.6
Fe, Expt. [62] [†]	1113	n/a	disord.	C^T	147	116	100	15	6.6	126	49	129	0.33	2.6
	1133	n/a	disord.	C^T	145	116	100	15	6.8	125	48	127	0.33	2.6
Fem Expt. [63] [‡]	1043	n/a	disord.	C^T	189	157	107	16	7.0	168	52	140	0.36	3.2
	1173	n/a	disord.	C^T	190	166	118	12	11.7	174	51	139	0.37	3.4

[§] Impulse excitation technique. Data were read from figure and converted to isothermal coefficients.

[†] Ultrasonic measurement. Data were converted to isothermal coefficients, and VRH averaging was applied.

[‡] Neutron scattering with a Born-von Kármán model. VRH averaging was applied.

4.2. Temperature-dependent elastic properties of reduced activation steels

The elastic properties of the three reduced activation steels are similar in both their magnetically ordered and paramagnetic states (Table 1) due to similar chemical composition. We thus expect that the elastic parameters of these alloys exhibit similar temperature dependences, and investigated these only for CLAM steel.

Fig. 2 shows the isothermal single-crystal elastic constants of CLAM steel in the temperature interval of 0–1120 K. The derived polycrystalline moduli are shown in Fig. 3. We find that C_{11}^T and C^T decrease monotonically and strongly with increasing temperature below T_{ord}. In contrast, C_{12}^T and C_{44}^T are with a maximum variation of less than 10 GPa nearly stable with temperature. Upon approaching the Curie temperature from below, the rates of change of C_{11}^T and C^T, and to a lesser extent also C_{44}^T, increase. The Zener anisotropy exhibits a significant increase with temperature. In passing through the ordering temperature, all $C_{\alpha\beta}^T$ show clear kinks. Above the magnetic transition, the rate of change of all the elastic constants is significantly lower than slightly below T_{ord}, and mainly determined by volume expansion only.

B^T, G^T, and E^T of CLAM decrease with increasing temperature. The B^T/G^T and ν^T have similar trends versus temperature: they are virtually invariant in the interval of 0–600 K, exhibit a progressively increasing trend between approximately 600 K and T_{ord}, and show a weak decrease in the paramagnetic phase up to 1120 K.

In order to clarify the alloying effects, theoretical results for bcc Fe are also shown in Figs. 2 and 3. The elastic constants of pure Fe show an overall temperature dependence similar to CLAM steel. Specifically, we find a pronounced softening of C_{11}^T and C^T, which accelerates upon approaching the ordering temperature. C_{12}^T and C_{44}^T are with a maximum variation of less than 10 GPa nearly stable with temperature. A notable difference is that B^T/G^T and ν^T of Fe show non-monotonic trends in the partially magnetically disordered domain.

Section 5.3 discusses a technical issue with obtaining precise theoretical values for C_{11}^T, C_{12}^T, and B^T for pure Fe below about 350 K, which is responsible, at least in parts, for the non-monotonic temperature trends determined in the low-temperature region.

5. Discussion

This work has explored the effect of temperature on the elastic parameters of reduced activation steels. In what follows, we first discuss how above model results compare with experimental observations. Second, we discuss the relative importance of the partial contributions to the temperature dependences of the elastic parameters. In the third part, we analyze the effects of chemical alloying and magnetic disordering on a peculiar magneto-volume phenomenon appearing on the equation of state in pure Fe, and discuss its consequences for an accurate equation of state fitting.

5.1. Comparison with experimental observations

The model results are compared with experimental elastic parameters for reduced activation steels. Since the available literature data is limited to two polycrystalline moduli, we include the single-crystalline elastic constants and polycrystalline moduli of pure Fe in the model validation. This also enables comparison of the theoretical and experimental alloying effects.

Tripathy et al. determined the isentropic shear and Young's moduli for the ferritic phase of a reduced activation ferritic/martensitic steel (referred to as RAFM hereafter) by a resonant impulse excitation technique (IET) [64]. The effective chemical composition of the RAFM steel, $Fe_{0.8914}Cr_{0.0974}W_{0.0030}V_{0.0025}Mn_{0.0057}$, is similar to that of the CLAM steel, when a total of 0.6 at.% minor alloying elements is neglected. Although the microstructure of the RAFM steel contained a small volume fraction of carbides, Tripathy et al. reasoned that the elastic properties of the ferrite + carbide phase do not differ much from the pure ferritic phase.

For a useful comparison with the theoretical isothermal elastic constants, we converted the isentropic experimental values [64] using experimental data for the thermal expansion of CLAM (Fig. 1) and, due to lack of data, the heat capacity of Fe [65,66]. Using the heat capacity of Fe is justified since differences between the heat capacities of Fe and RAFM steel are expected to result in less than 1 GPa difference between the isothermal and isentropic Young's moduli, which is largest deviation between these moduli we determined for pure Fe. For ease of comparison, the converted data for the RAFM steel in the temperature domain of 298 to ~1100 K was added to Fig. 3 and ~1100 K data to Table 1.

As is evident, the theoretical G^T and E^T systematically overestimate the experimental values. The agreement is the closest at ~400 K (15% overestimation) and the least satisfactory in the paramagnetic state (30% and 40% for G^T and E^T, respectively). The theoretical temperature dependences of both moduli for CLAM are qualitatively consistent with the converted IET data for RAFM, but quantitative differences in the temperature dependence of the slopes occur, both below and above T_{ord}. Whereas the experimental G^T and E^T show minor anomalies in passing through the Curie temperature, the present theoretical results show clear kinks at the (theoretical) Curie temperature. The kinks in the model predictions are attributed to the magnetic energy (cf. discussion in Sec. 5.2). In this context it should be realized that ζ
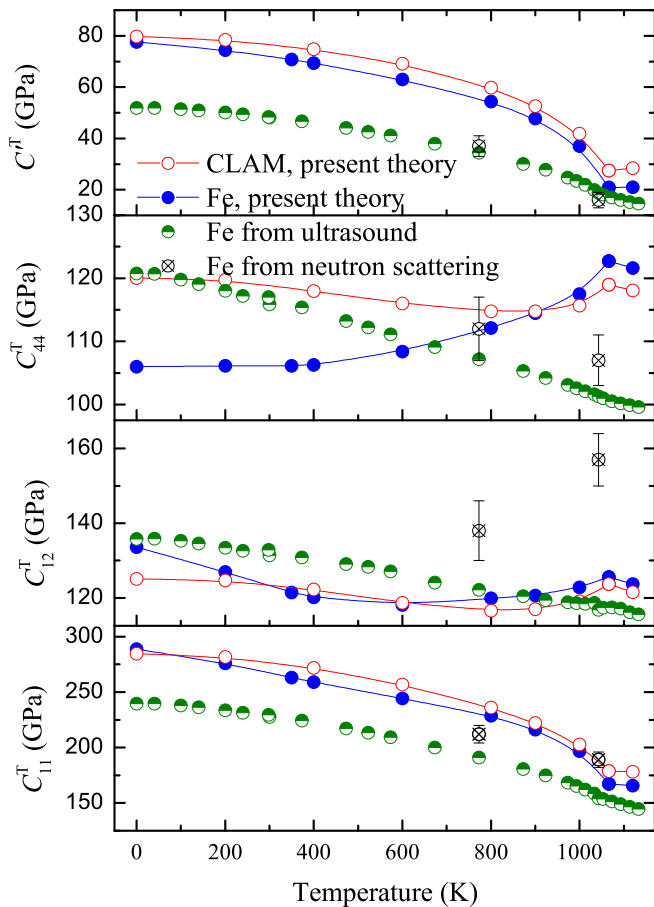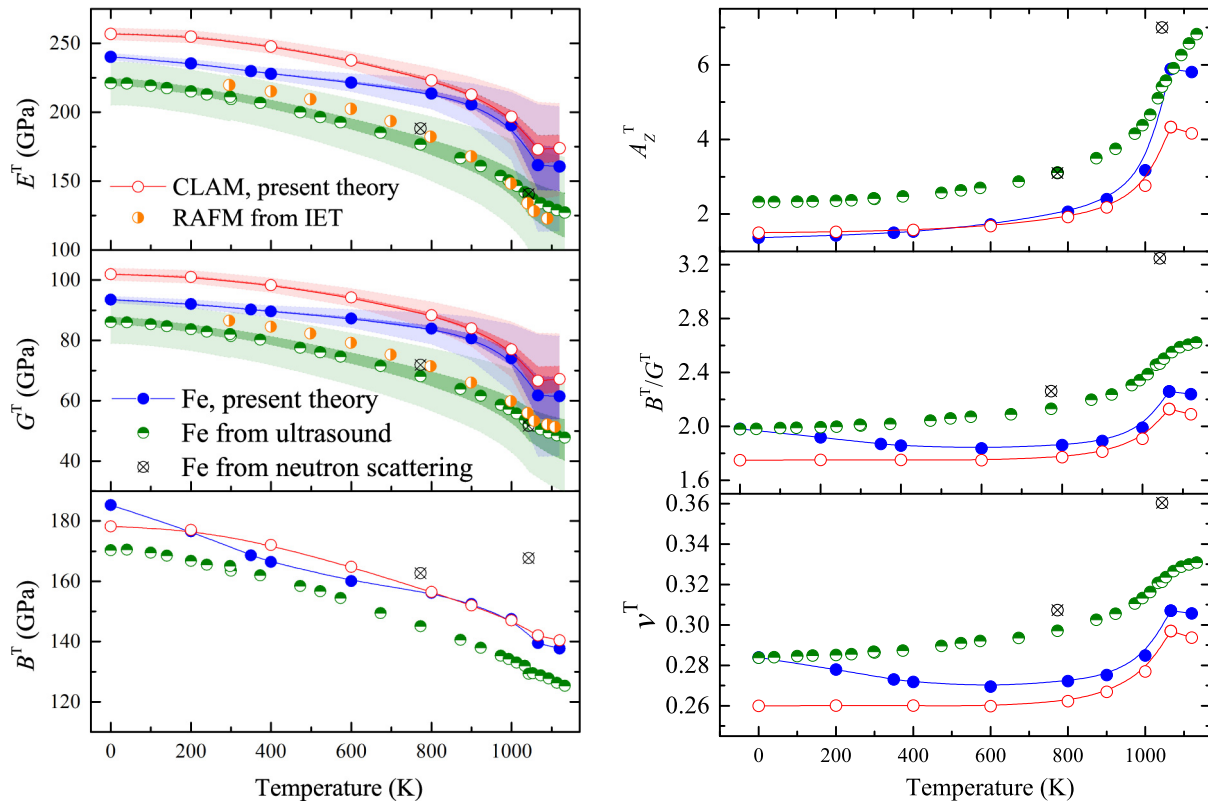

Fig. 2. Isothermal single-crystal elastic constants of CLAM from present theory as a function of temperature. Present theoretical data and experimental data [61–63] for Fe are shown for reference. The experimental data were determined from ultrasonic methods [61,62] and converted to isothermal coefficients, or neutron scattering [63]. Lines guide the eye and the legend applies to all panels.

Fig. 3. Isothermal polycrystalline elastic moduli and Zener anisotropy of CLAM from present theory and experimental data for the ferritic phase of an RAFM steel [64] (from IET, read from figure, converted to isothermal coefficients) as a function of temperature. Present theoretical data and experimental data [61–63] for Fe are shown for reference. The experimental data for Fe were obtained through VRH averaging from the single-crystal data measured by ultrasound [61,62] (after conversion to isothermal coefficients) or neutron scattering [63]. The markers correspond to Hill averages or experimental data. The colored, shaded regions with high transparency correspond to the Voigt and Reuss bounds on E^T and G^T, those with low transparency correspond to the tighter, Hashin-Shtrikman bounds. Lines guide the eye and the legend applies to all panels.

increases rapidly just below T_{ord} (cf. Sec. 3.4). Besides, residual magnetic short-range order [67,68] and longitudinal spin fluctuations above the ordering temperature, which are not considered in the present model, are suggested to account for part of the deviation.

To measure the performance of the theoretical predictions for CLAM steel, we extend the comparison between theory and experiment by considering experimental single-crystal elastic constants of Fe, which were either derived from ultrasonic measurements [61,62] and resemble to a larger extent isentropic elastic constant, or neutron scattering (Born-von Kármán model fitted to phonon dispersion relations) [63]. We converted the isentropic coefficients to isothermal coefficients using the heat capacity [65,66] and thermal expansion of Fe [43]. We estimated the isothermal elastic moduli through VRH averaging. For ease of comparison, these data for Fe was added to Figs. 2 and 3, and Table 1.

In the paramagnetic state, the present theory gives 10–21% larger values for C_{11}^T, C_{12}^T and C_{44}^T and a 12% lower Zener anisotropy in comparison to the ultrasonic data [62]. The three polycrystalline moduli are overestimated to similar degree. In comparison to the neutron scattering data from Ref. [63], the present results, however, underestimate C_{11}^T, C_{12}^T, and B^T. The effect of temperature on the strongly temperature-dependent C_{11}^T and C'^T is well captured by our model. The model does not satisfactorily capture the weak decreases of C_{12}^T and C_{44}^T with temperature. The incorrect theoretical trend for C_{44}^T follows from the fact that this parameter is larger in the paramagnetic phase than in the ferromagnetic state at zero temperature, attributed to a failure of semi-local exchange-correlation functionals [15,69]. The effect of temperature on the derived polycrystalline moduli and Zener anisotropy is reproduced, as their variation with temperature is mainly

determined by the strongly temperature-dependent elastic constants. The present theoretical temperature dependences for pure Fe are similar to those published previously (C', C_{44}, B, A_Z) [15], despite methodological differences.

Lastly, we compare the theoretical and experimental alloying effects on E^T and G^T. We recall that the experimental moduli for Fe are effective moduli, which we estimated through VRH averaging, whereas the experimental values for the RAFM steel are for bulk polycrystals. We thus account for bounds on the effective moduli of Fe. We find from Fig. 3 that E^T and G^T of the RAFM steel lie within the Voigt and Reuss bounds on the effective moduli of Fe for all considered temperatures. That is, definite answers on the experimental alloying trend are difficult owing to the width of Voigt and Reuss bounds. However, using the tighter Hashin-Shtrikman bounds for the effective moduli of Fe, E^T and G^T of RAFM are larger than the corresponding upper bound for Fe below ~850 K and lie within the Hashin-Shtrikman bounds for temperatures above. That is, the theoretical and experimental alloying effects are consistent below ~850 K, whereas definite conclusions on the alloying trend above that temperature are difficult.

Contrasting the theoretical and experimental temperature trends for CLAM and Fe, we conclude that the present theoretical approach has similar performance in the case of complex alloys as for pure bcc Fe. The deviations are mainly due to basic DFT errors (exchange-correlation approximation) or the neglect of magnetic short range order in the paramagnetic regime. More importantly, the experimentally detected alloying trends are well reproduced by our theory especially at temperatures up to slightly below the magnetic transition temperature.

5.2. Significance of partial contributions to temperature dependence of elastic parameters

In what follows we disentangle the partial contributions from volume expansion and magnetism to the temperature-dependent elastic parameters of the reduced activation steels to discuss their relative importance. The effect of loosing complete long-range magnetic order can be isolated by contrasting the above results (Table 1) in the magnetically ordered and paramagnetic states for invariant volume and temperature. On the other hand, the combined effect of volume expansion and entropy can be separated out by comparing the paramagnetic results for the two tabulated volume-temperature pairs.

As is evident, the relative significance of long-range magnetic order and the combined effect of volume expansion and entropy varies starkly with elastic parameter. Neither of these two partial contributions has a dominating effect on the temperature dependence. Specifically, the absence of long-range magnetic order reduces C_{11}^T and C^T and increases C_{12}^T and C_{44}^T relative to the magnetically ordered state. Volume expansion and entropy decreases C_{11}^T, C_{12}^T, and C_{44}^T, whereas C^T remains nearly invariant. Thus, the total temperature effect on C^T primarily originates from loss of long-range magnetic order. Volume expansion and entropy fully and partially override, respectively, the increasing trend set by the loss of long-range magnetic order for C_{12}^T and C_{44}^T, whereas both partial contributions reinforce each other in the case of C_{11}^T. We note that similar conclusions are reached for the effective moduli. Furthermore, analysis of our data showed that volume expansion gives a larger contribution than magnetic entropy.

The regular temperature dependence (mainly due to explicit lattice contributions and volume expansion) of the three cubic elastic constant C_{11}, C_{12}, and C_{44} in nonmagnetic metals is a power-law dependence on T at very low temperatures and a linear decrease with T at high temperatures [70]. Assuming that Fe and CLAM steel in the *paramagnetic* state follows this regular behavior (volume expansion and entropy were shown to lead to a quasi-linear dependence of C_{44}^T in iron [15]), the pronounced non-linearities observed in the ferromagnetic region (Fig. 2, theoretical data) are attributed to the loss of long-range magnetic order. This is consistent with Dever's reasoning [62] that the nonlinear temperature dependence of the measured single-crystal elastic constants in Fe is associated with the degree of ferromagnetic ordering.

5.3. Stability of the bulk modulus from EOS fitting

Commonly employed EOSs (e.g., Morse, Murnaghan, Birch-Murnaghan) applied to ferromagnetic bcc Fe yield values of the bulk modulus that are unusually sensitive to the fitting interval chosen [71]. The underlying, physical reason is a rapid change of the magnetic moment occurring at volumes slightly above the theoretical equilibrium volume, the effect of which on the total energy-volume data is not correctly captured by these common EOSs. Including these volumes in the fit (unintentionally or not) tends to underestimate the bulk modulus of Fe and yields a poor goodness of fit compared to excluding the larger volumes.

Whether the same issue applies to Fe at finite temperature and CLAM steel, and its significance for the derived single-crystal elastic constants, is discussed in the following. In order to distinguish any influence of the physical effect mentioned above on the quality of fit from a typical error associated with least squares EOS fitting (which includes, for instance, numerical errors), we estimate the mean squared error (MSE, also chi-squared per degree of freedom),

$$\text{MSE} = \frac{\sum_{n=1}^{N} \left(F_{\text{mag}}^{(n)}(T, \mathbf{0}, \zeta) - F_{\text{EOS}}^{(n)} \right)^2}{N - p}. \tag{11}$$

Here, $N - p$ is the number of degrees of freedom, N the number of free energy-volume data points at a temperature T, p the number of

parameters [$p = 4$ for all EOSs mentioned here (bulk modulus and its pressure derivative, volume, and energy at equilibrium)]. F_{EOS} refers to the EOS fitted. We also deemed that a scatter of the bulk modulus in the order of 2 GPa over the different interval widths considered is an appropriate and acceptable theoretical error.

Fig. 4(a) shows the isothermal bulk moduli of Fe and CLAM steel in the temperature interval of 0–600 K obtained by fitting the Birch-Murnaghan EOS to free energy data in five different interval widths. The lower boundary is identical to 2.58 Bohr in each case, while the upper boundary is gradually extended. The step size is 0.02 Bohr in each case. Fig. 4(b) shows the corresponding MSEs.

It is obvious that the bulk moduli of Fe scatter significantly at zero temperature (≈ 13 GPa), 200 K (≈ 8 GPa), and 350 K (≈ 3 GPa) over the interval widths considered. At 400 K and 600 K, the difference between the largest and smallest value is ≤ 2 GPa. In contrast, the scatter of the bulk moduli for CLAM amounts to ≤ 1 GPa at any of the temperatures considered. Note that for the sake of clarity, only a single curve for CLAM steel is shown in Fig. 4(a), whereas the size of the symbols represents the scatter of B^T over the five interval widths.

Using other common EOSs (Morse, Murnaghan, Vinet, and Poirier-Tarantola), we found that these EOSs lead to very similar results as shown in Fig. 4(a) for the Birch-Murnaghan EOS.

The fitting to a narrower interval is accompanied by a smaller MSE [Fig. 4(b), Fe data], thus an improved goodness of fit. For the data at 600 K (small scatter of B^T), the MSE for the interval of 2.58–2.70 Bohr is approximately 10 times smaller than that of 2.58–2.80 Bohr, but it is approximately a 100 times smaller at 0 K (large scatter of B^T). The interval of 2.58–2.70 Bohr has the smallest MSEs. We recall that this interval was the default setting employed to obtain all results presented in Sec. 4. For CLAM, we found that $1 \cdot 10^{-10} \leq \text{MSE} \leq 1 \cdot 10^{-8}$ eV^2 (typically the smallest MSE occurred for the widest interval), and one representative case is shown in Fig. 4(b).

These results confirm the finding from Zhang et al. [71] that including large Wigner-Seitz radii in the EOS fit tends to decrease the bulk modulus of Fe at zero temperature. By doing so, the theoretical and experimental values can be brought near coincidence [see Fig. 4(a)], but results in a poorer goodness of fit. Besides, we find the same effect on B^T in our finite temperature calculations below approximately 350 K, although a systematic overestimation of the experimental value remains.

Fig. 4(c) shows an increasing magnetization (magnetic moment per site) with Wigner-Seitz radius for both Fe and CLAM steel. An increasing trend for Fe is expected from a band theory point of view. Interestingly, in the magnetically ordered state, the magnetic moment of pure Fe exhibits a rapid transition between 2.70 and 2.74 Bohr due to a band structure effect near the Fermi level [71]. A similar, but diminished change in the moment between 2.70 and 2.74 Bohr occurs for Fe at 200 and 400 K, whereas no such feature appears on the 600 K curve. We recall that the higher the temperature, the larger the pseudo-alloy concentration. Thus, the rapid transition is gradually removed due to magnetic disorder (i.e., pseudo-alloying) effects on the electronic states. The transition is completely absent in paramagnetic Fe (not shown) and CLAM steel irrespective of temperature/magnetic state [zero Kelvin magnetically ordered state is shown in Fig. 4(c)]. In the case of CLAM steel, the high Cr content (chemical composition close to Fe$_{0.9}$Cr$_{0.1}$) induced strong disorder effects in the majority spin channel near the Fermi level, where electronic states loose their band character, but largely preserves their band character in the minority spin channel [72].

As is evident, the smoothing of the magnetic moment curve with temperature, the decrease of the scatter in the bulk modulus (at fixed temperature) over extending the fitting interval, and the improvement of the goodness of fit appear simultaneously. The common EOSs accurately fit the free energy-volume data when the physical reason for the deviation disappears, i.e., magnetic and/or alloy disorder effects remove the rapid change of the magnetic moment occurring at volumes slightly above the theoretical equilibrium volume.
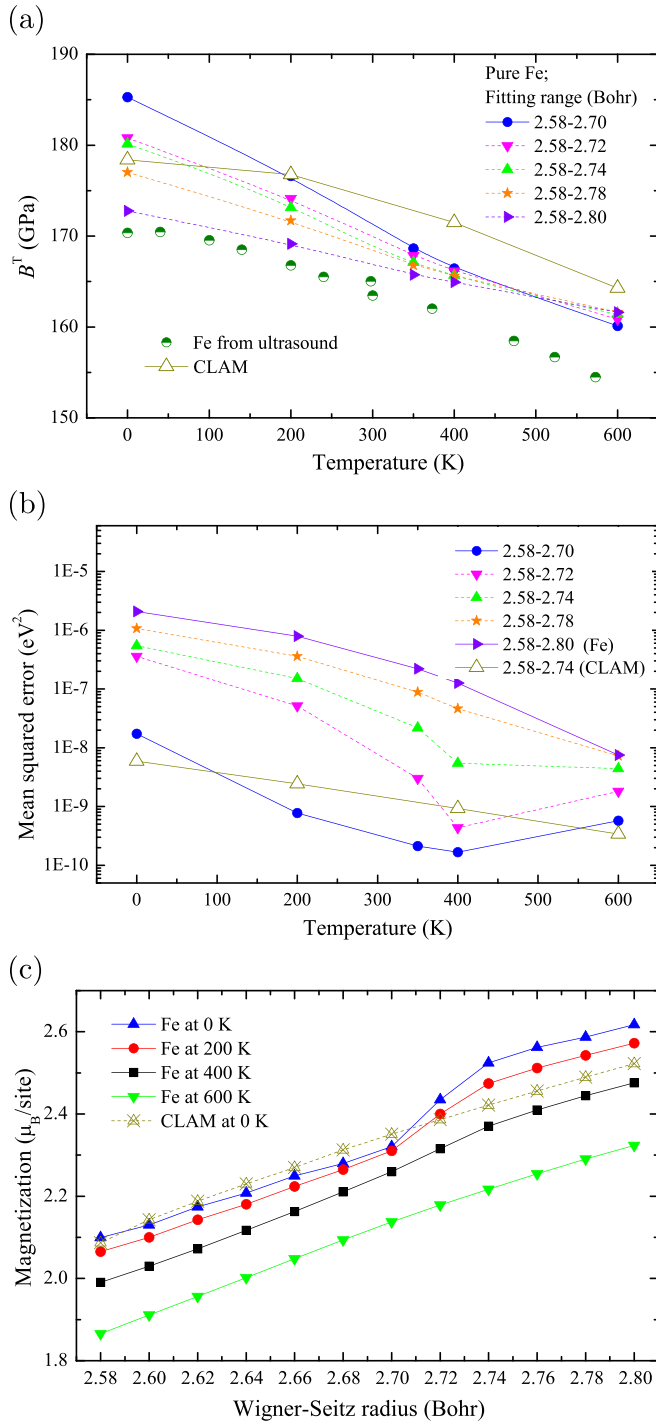
Fig. 4. (a) Isothermal bulk moduli of Fe and CLAM steel versus temperature obtained from fitting the Birch-Murnaghan EOS to free energy data in varying interval widths as indicated in the legend (Wigner-Seitz radii). For the sake of clarity, only a single curve for CLAM steel is shown, where the size of the symbols represent the scatter of B^T over the five interval widths (≤ 1 GPa). The experimental data for Fe were determined from ultrasonic methods [61,62] and converted to isothermal coefficients. (b) MSEs of the least squares EOS fit corresponding to (a). (c) Magnetization of Fe and CLAM steel in the magnetically ordered states at zero temperature, and of Fe for various degrees of partial magnetic disorder indicated by the temperature as a function of the Wigner-Seitz radius. Lines guide the eye.

The scatter of B^T with interval width leads to equal changes in C_{11}^T and C_{12}^T derived from B^T, since

$$C_{11}^T = B^T + \frac{4}{3}C'^T \quad \text{and} \tag{12}$$

$$C_{12}^T = B^T - \frac{2}{3}C'^T. \tag{13}$$

As is evident from Fig. 1, a smaller B^T for bcc Fe (e.g., due to including large Wigner-Seitz radii in the EOS fit) would reduce the overestimation of the experimental C_{11}^T and simultaneously lead to a more stable C_{12}^T with temperature.

An alternative strategy suggesting itself is to avoid any EOS fitting. To test this hypothesis, we derived the linear combination $C_{11} - C_{12}$ from the strain energy change for applied strain $\boldsymbol{\varepsilon} = \text{diag}\,(\varepsilon, -\varepsilon, 0)$ (all other settings were identical to those of determining C'^T). We obtained $B^T = 186$ GPa for Fe at zero temperature, which is virtually identical to the result obtained with the Birch-Murnaghan EOS.

6. Conclusions

The isothermal single-crystal and polycrystalline elastic parameters of three Fe-rich reduced activation steels, CLAM, F82H, and EUROFER97 (main alloying elements), have been determined in their magnetically ordered (0 K) and paramagnetic bcc phases (1120 K). The temperature dependence ($T \leq 1120$ K) of these micro-mechanical properties has been investigated for CLAM based on a finite-temperature modeling approach.

Based on the results obtained the following important conclusions are drawn:

(i) The assessment for a RAFM steel shows that the model approach captures the effect of temperature on the available data for E^T and G^T. In the case of Fe, the effect of temperature on the strongly temperature-dependent elastic constants C_{11}^T and C'^T, and the derived polycrystalline moduli and Zener anisotropy is reproduced. The weak changes of C_{12}^T and C_{44}^T with temperature do not follow the experimental trends.

(ii) Relative to pure Fe, the effects of the main alloy additions characteristic of the three reduced activation steels on the elastic properties differ in the magnetically ordered and disordered phases.

(iii) Contributions due to loss of long-range magnetic order and the combined effect of volume expansion and entropy are important in determining the temperature dependence of the elastic parameters in all the materials investigated. The relative significance of the two partial contributions is specific to each elastic constant, but similar in the reduced activation steels and Fe.

(iv) The bulk modulus of Fe below about 350 K was found to be unusually sensitive to the fitting interval chosen in fitting with common EOSs. The effect is absent in CLAM. The large sensitivity was ascribed to a rapid change of the magnetic moment on volume increase, the effect of which on the energy is not captured by common EOSs. Similar effects may exist in other itinerant magnets. This is important since erroneous EOS fitting should be avoided in order to assess the performance of common exchange-correlation functionals in predicting basic ground-state properties.

Declaration of Competing Interest

The authors declare that they have no known competing financial interests or personal relationships that could have appeared to influence the work reported in this paper.

Acknowledgments

References

[1] R. Klueh, A. Nelson, Ferritic/martensitic steels for next-generation reactors, J. Nucl. Mater. 371 (1) (2007) 37–52.

[2] A. Ruiz-Moreno, P. Hähner, Indentation size effects of ferritic/martensitic steels: a comparative experimental and modelling study, Mater. Des. 145 (2018) 168–180.

[3] I. Cook, Materials research for fusion energy, Nat. Mater. 5 (2) (2006) 77.

[4] F. Roters, P. Eisenlohr, L. Hantcherli, D. Tjahjanto, T. Bieler, D. Raabe, Overview of constitutive laws, kinematics, homogenization and multiscale methods in crystal plasticity finite-element modeling: theory, experiments, applications, Acta Mater. 58 (4) (2010) 1152–1211.

[5] D. Wei, X. Li, S. Schönecker, J. Jiang, W.-M. Choi, B.-J. Lee, H.S. Kim, A. Chiba, H. Kato, Development of strong and ductile metastable face-centered cubic single-phase high-entropy alloys, Acta Mater. 181 (2019) 318–330.

[6] H.K. Yeddu, A. Malik, J.Å. Gren, G. Amberg, A. Borgenstam, Three-dimensional phase-field modeling of martensitic microstructure evolution in steels, Acta Mater. 60 (4) (2012) 1538–1547.

[7] A.S. Argon (Ed.), Topics in Fracture and Fatigue, Springer, New York, 1992.

[8] X. Li, W. Li, D.L. Irving, L.K. Varga, S. Schönecker, Ductile and brittle crack-tip response in equimolar refractory high-entropy alloys, Acta Mater. 189 (2020) 174–187.

[9] A.S. Argon, Strengthening Mechanisms in Crystal Plasticity, Oxford University Press, New York, 2008.

[10] G. Qin, R. Chen, P.K. Liaw, Y. Gao, L. Wang, Y. Su, H. Ding, J. Guo, X. Li, An as-cast high-entropy alloy with remarkable mechanical properties strengthened by nanometer precipitates, NANOSCALE 12 (6) (2020) 3965–3976, https://doi.org/10.1039/c9nr08338c.

[11] J.P. Hirth, J. Lothe, Theory of Dislocations, 2nd edition Wiley, New York, 1982.

[12] T. Moriya, Spin Fluctuations in Itinerant Electron Magnetism, Springer, Berlin Heidelberg, 1985.

[13] K. Baberschke, M. Donath, W. Nolting (Eds.), Band-Ferromagnetism: Ground State and Finite-Temperature Phenomena, Vol. 580 of Lecture notes in physics, Springer, Berlin Heridelberg, 2001.

[14] F. Körmann, A. Dick, B. Grabowski, B. Hallstedt, T. Hickel, J. Neugebauer, Free energy of bcc iron: integrated ab initio derivation of vibrational, electronic, and magnetic contributions, Phys. Rev. B 78 (2008), 033102, .

[15] V.I. Razumovskiy, A.V. Ruban, P.A. Korzhavyi, Effect of temperature on the elastic anisotropy of pure Fe and $Fe_{0.9}Cr_{0.1}$ random alloy, Phys. Rev. Lett. 107 (20) (2011) 205504.

[16] F. Körmann, B. Grabowski, B. Dutta, T. Hickel, L. Mauger, B. Fultz, J. Neugebauer, Temperature dependent magnon-phonon coupling in bcc Fe from theory and experiment, Phys. Rev. Lett. 113 (2014) 165503.

[17] N. Baluc, D. Gelles, S. Jitsukawa, A. Kimura, R. Klueh, G. Odette, B. van der Schaaf, J. Yu, Status of reduced activation ferritic/martensitic steel development, J. Nucl. Mater. 367–370 (Part A) (2007) 33–41.

[18] Q. Huang, N. Baluc, Y. Dai, S. Jitsukawa, A. Kimura, J. Konys, R. Kurtz, R. Lindau, T. Muroga, G. Odette, B. Raj, R. Stoller, L. Tan, H. Tanigawa, A.-A. Tavassoli, T. Yamamoto, F. Wan, Y. Wu, Recent progress of R&D activities on reduced activation ferritic/martensitic steels, J. Nucl. Mater. 442 (1–3, Supplement 1) (2013) S2–S8.

[19] X. Li, X. Li, S. Schönecker, R. Li, J. Zhao, L. Vitos, Understanding the mechanical properties of reduced activation steels, Mater. Des. 146 (2018) 260–272.

[20] D.C. Wallace, Solid state physics - advances in research and applications, Ch. Thermoelastic Theory of Stressed Crystals and Higher-Order Elastic Constants, Vol. 25, Academic Press Inc 1970, pp. 301–404.

[21] J. Wang, J. Li, S. Yip, S. Phillpot, D. Wolf, Mechanical instabilities of homogeneous crystals, Phys. Rev. B 52 (1995) 12627–12635.

[22] R.F.S. Hearmon, The elastic constants of anisotropic materials, Rev. Mod. Phys. 18 (1946) 409–440.

[23] G. Davies, Effective elastic moduli under hydrostatic stress – I. quasi-harmonic theory, J. Phys. Chem. Solids 35 (11) (1974) 1513–1520.

[24] L.D. Landau, E.M. Lifschitz, Elastizitätstheorie, Lehrbuch der Theoretischen Physik, 6th edition, Vol. 7, Akademie-Verlag, Berlin, 1989.

[25] R. Hill, The elastic behaviour of a crystalline aggregate, Proc. Phys. Soc. Lond. A 65 (5) (1952) 349.

[26] Z. Hashin, S. Shtrikman, A variational approach to the elastic behavior of multiphase materials, J. Mech. Phys. Solids 11 (1962) 127–10.

[27] A.J. Pindor, J. Staunton, G.M. Stocks, H. Winter, Disordered local moment state of magnetic transition metals: a self-consistent KKR CPA calculation, J. Phys. F. 13 (1983) 979–989.

[28] J. Staunton, B.L. Györffy, A.J. Pindor, G.M. Stocks, H. Winter, Electronic structure of metallic ferromagnets above the Curie temperature, J. Phys. F. 15 (1985) 1387–1404.

[29] B. Gyorffy, A. Pindor, J. Staunton, G. Stocks, H. Winter, A first-principles theory of ferromagnetic phase transitions in metals, J. Phys. F. 15 (6) (1985) 1337.

[30] H. Akai, P.H. Dederichs, Local moment disorder in ferromagnetic alloys, Phys. Rev. B 47 (1993) 8739–8747.

[31] S. Khmelevskyi, I. Turek, P. Mohn, Large negative magnetic contribution to the thermal expansion in iron-platinum alloys: quantitative theory of the invar effect, Phys. Rev. Lett. 91 (2003), 037201, .

[32] G. Grimvall, Polymorphism in metals II. Electronic and magnetic free energy, Phys. Scr. 12 (3) (1975) 173.

[33] S. Schönecker, X. Li, B. Johansson, S. Kwon, L. Vitos, Thermal surface free energy and stress of iron, Sci. Rep. 5 (2015) 14860, https://doi.org/10.1038/srep14860.

[34] N.D. Mermin, Thermal properties of the inhomogeneous electron gas, Phys. Rev. 137 (1965) A1441–A1443.

[35] K. Wildberger, P. Lang, R. Zeller, P.H. Dederichs, Fermi-Dirac distribution in ab initio Green's-function calculations, Phys. Rev. B 52 (1995) 11502.

[36] N.M. Rosengaard, B. Johansson, Finite-temperature study of itinerant ferromagnetism in Fe, Co, and Ni, Phys. Rev. B 55 (1997) 14975–14986.

[37] L. Bergqvist, A. Bergman, Realistic finite temperature simulations of magnetic systems using quantum statistics, Phys. Rev. Mater. 2 (2018), 013802, .

[38] M.D. Kuźmin, Shape of temperature dependence of spontaneous magnetization of ferromagnets: quantitative analysis, Phys. Rev. Lett. 94 (10) (2005) 107204.

[39] X. Li, S. Schönecker, E. Simon, L. Bergqvist, H. Zhang, L. Szunyogh, J. Zhao, B. Johansson, L. Vitos, Tensile strain-induced softening of iron at high temperature, Sci. Rep. 5 (2015) 16654, https://doi.org/10.1038/srep16654.

[40] K. Sato, L. Bergqvist, J. Kudrnovský, P.H. Dederichs, O. Eriksson, I. Turek, B. Sanyal, G. Bouzerar, H. Katayama-Yoshida, V.A. Dinh, T. Fukushima, H. Kizaki, R. Zeller, First-principles theory of dilute magnetic semiconductors, Rev. Mod. Phys. 82 (2010) 1633–1690.

[41] W. Xiong, P. Hedström, M. Selleby, J. Odqvist, M. Thuvander, Q. Chen, An improved thermodynamic modeling of the Fe-Cr system down to zero kelvin coupled with key experiments, Calphad 35 (3) (2011) 355–366.

[42] E. Grüneisen, Handbuch der Physik, vol. 10, Springer, Berlin, 1926 1.

[43] F. Nix, D. MacNair, The thermal expansion of pure metals: copper, gold, aluminum, nickel, and iron, Phys. Rev. 60 (8) (1941) 597.

[44] X. Li, Materials for advanced energy technology from quantum-mechanical modeling, Ph.D. thesis, KTH Stockholm, 2020.

[45] F.C. Hull, S.K. Hwang, J.M. Wells, R.I. Jaffee, Effect of composition on thermal expansion of alloys used in power generation, J. Mater. Sci. 9 (1) (1987) 81–92.

[46] X. Li, H. Zhang, S. Lu, W. Li, J. Zhao, B. Johansson, L. Vitos, Elastic properties of vanadium-based alloys from first-principles theory, Phys. Rev. B 86 (2012), 014105, .

[47] F. Birch, Finite elastic strain of cubic crystals, Phys. Rev. 71 (11) (1947) 809.

[48] Lectures on methods of electronic structure calculations, in: V. Kumar, O.K. Andersen, A. Mookerjee (Eds.), Ch. Exact Muffin-Tin Theory, World Scientific, Singapore 1994, pp. 63–124.

[49] L. Vitos, Total-energy method based on the exact muffin-tin orbitals method, Phys. Rev. B 64 (1) (2001), 014107, .

[50] L. Vitos, H.L. Skriver, B. Johansson, J. Kollár, Application of the exact muffin-tin orbitals theory: the spherical cell approximation, Comput. Mater. Sci. 18 (1) (2000) 24–28.

[51] J.P. Perdew, Y. Wang, Accurate and simple analytic representation of the electron-gas correlation energy, Phys. Rev. B 45 (23) (1992) 13244–13249.

[52] L. Vitos, J. Kollár, H.L. Skriver, Full charge-density scheme with a kinetic-energy correction: application to ground-state properties of the 4d metals, Phys. Rev. B 55 (1997) 13521.

[53] J.P. Perdew, K. Burke, M. Ernzerhof, Generalized gradient approximation made simple, Phys. Rev. Lett. 77 (18) (1996) 3865.

[54] B.L. Györffy, Coherent-potential approximation for a nonoverlapping-muffin-tin-potential model of random substitutional alloys, Phys. Rev. B 5 (6) (1972) 2382–2384.

[55] A. Taga, L. Vitos, B. Johansson, G. Grimvall, Ab initio calculation of the elastic properties of $Al_{1−x}Li_x$ ($x \le 0.20$) random alloys, Phys. Rev. B 71 (2005), 014201, .

[56] L. Vitos, I.A. Abrikosov, B. Johansson, Anisotropic lattice distortions in random alloys from first-principles theory, Phys. Rev. Lett. 87 (15) (2001) 156401.

[57] P.A. Korzhavyi, A.V. Ruban, I.A. Abrikosov, H.L. Skriver, Madelung energy for random metallic alloys in the coherent potential approximation, Phys. Rev. B 51 (9) (1995) 5773.

[58] A.V. Ruban, H.L. Skriver, Screened coulomb interactions in metallic alloys. I. universal screening in the atomic-sphere approximation, Phys. Rev. B 66 (2) (2002) 024201.

[59] Z. Dong, W. Li, D. Chen, S. Schönecker, M. Long, L. Vitos, Longitudinal spin fluctuation contribution to thermal lattice expansion of paramagnetic Fe, Phys. Rev. B 95 (2017), 054426, .

[60] Z. Dong, W. Li, S. Schönecker, S. Lu, D. Chen, L. Vitos, Thermal spin fluctuation effect on the elastic constants of paramagnetic Fe from first principles, Phys. Rev. B 92 (22) (2015) 224420.

[61] J.J. Adams, D. Agosta, R. Leisure, H. Ledbetter, Elastic constants of monocrystal iron from 3 to 500 K, J. Appl. Phys. 100 (11) (2006) 113530.

[62] D. Dever, Temperature dependence of the elastic constants in α-iron single crystals: relationship to spin order and diffusion anomalies, J. Appl. Phys. 43 (8) (1972) 3293–3301.

[63] J. Neuhaus, M. Leitner, K. Nicolaus, W. Petry, B. Hennion, A. Hiess, Role of vibrational entropy in the stabilization of the high-temperature phases of iron, Phys. Rev. B 89 (2014) 184302.

[64] H. Tripathy, S. Raju, R.N. Hajra, S. Saibaba, High temperature elastic properties of reduced-activation ferritic-martensitic (RAFM) steel using impulse excitation technique, Metall. Mater. Trans. A 49 (2018) 979–989, https://doi.org/10.1007/s11661-017-4449-3.

[65] D.C. Wallace, P.H. Sidles, G.C. Danielson, Specific heat of high purity iron by a pulse heating method, J. Appl. Phys. 31 (1960) 168–176.

[66] T.S. Touloukian, E.H. Buyco, Thermophysical Properties of Matter, vol. 4, IFI/Plenum, New York-Washington, 1970.

[67] V. Heine, R. Joynt, Coarse-grained magnetic disorder above T_c in iron, Europhys. Lett. 5 (1988) 81.

[68] G. Grimvall, Spin disorder in paramagnetic fcc iron, Phys. Rev. B 39 (1989) 12300.

[69] H. Zhang, M.P.J. Punkkinen, B. Johansson, L. Vitos, Elastic parameters of paramagnetic iron-based alloys from first-principles calculations, Phys. Rev. B 85 (5) (2012), 054107, .

[70] Y.P. Varshni, Temperature dependence of the elastic constants, Phys. Rev. B 2 (1970) 3952–3958.

[71] H.L. Zhang, S. Lu, M.P.J. Punkkinen, Q.-M. Hu, B. Johansson, L. Vitos, Static equation of state of bcc iron, Phys. Rev. B 82 (13) (2010) 132409.

[72] P.A. Korzhavyi, A.V. Ruban, J. Odqvist, J.-O. Nilsson, B. Johansson, Electronic structure and effective chemical and magnetic exchange interactions in bcc Fe-Cr alloys, Phys. Rev. B 79 (2009), 054202, .